Use of DBD plasma, photocatalysis, and combined DBD plasma/photocatalysis in a continuous annular reactor for isovaleraldehyde elimination - Synergetic effect and byproducts identification

Aymen Amine Assadi, Abdelkrim Bouzaza, Cédric Vallet, Dominique Wolbert

Use of DBD plasma, photocatalysis, and combined DBD plasma/photocatalysis in a continuous annular reactor for isovaleraldehyde elimination – synergetic effect and byproducts identification

Aymen Amine ASSADI [a,b], Abdelkrim BOUZAZA [a,b*], Cédric VALLET [c], Dominique WOLBERT [a,b],

[a] Laboratoire Sciences Chimiques de Rennes - équipe Chimie et Ingénierie des Procédés, UMR 6226 CNRS, ENSCR, 11 allée de Beaulieu, CS 50837, 35700 Rennes, France.

[b] Université Européenne de Bretagne, Rennes, France

[c] Ahlstrom Research and Services, ZI de l'Abbaye - Impasse Louis Champin - 38780 Pont-Evêque, France

* Corresponding author. Tel.: +33 2 23238056; fax: +33 2 23238120.

E-mail address: Abdelkrim.bouzaza@ensc-rennes.fr (A. Bouzaza).

Abstract

Removal of isovaleraldehyde from air was investigated experimentally by three processes: dielectric barrier discharge (DBD) plasma, photocatalysis and a DBD plasma/photocatalysis combination. The latter led to a synergetic effect.

Many operating parameters were investigated in this study such as the specific energy of discharge, the inlet concentration of isovaleraldehyde and the relative humidity. The UV light generated by the DBD plasma reactor did not activate the photocatalytic medium. Thus, its contribution to the removal of isovaleraldehyde by photocatalysis could be ignored. On the other hand, the use of external UV light significantly improved the removal efficiency.

Using a photocatalytic reactor in the presence of water vapor, in small amounts, had a promoting effect on the degradation due to the formation of $OH^{\bullet}$ radicals. The same phenomenon has been observed in other processes for small amounts of water in air.

The identified and analyzed byproducts were classified into four groups: intermediate products (propionic acid, acetic acid and acetone), carbon monoxide, carbon dioxide and ozone. The carbon balance on carbon products was achieved at about 90%.

Keywords:

Continuous reactor; synergetic effect; plasma-photocatalysis process; VOC removal; byproduct identification

1. Introduction

Odor pollution control is an important and challenging issue in the world. Therefore, the treatment of air pollutants has been widely studied during recent years **[1]**. Air pollution has become a major public concern in the last few decades. The main substances causing odor pollution are sulfur compounds (mercaptans, sulfides), nitrogen compounds (amines and ammonia), and many volatile organic compounds (VOCs) (fatty acids, aldehydes, ketones, alcohols, etc.) [**2**]. Many industries have seen their gas emissions controlled and limited for environmental reasons. Since 1979, each international protocol has fixed new regulations and gradually reduced the emission limit of major pollutants **[3]**.

To solve this problem, research has been conducted to find cost-effective approaches to reduce odor emissions [**4, 5**]. As a result, many conventional techniques have been proposed to remove VOCs, such as ozone oxidation [**6**], incineration **[3]** and photocatalysis [**7**]. This latter process is a promising air purification technology for trace contaminants because it can degrade a wide range of VOCs to H_2O and CO_2 at room temperature and atmospheric pressure **[8]**.

Recently, non-thermal plasma (NTP) has been investigated by many researchers for various applications such as methanol synthesis **[9]**, and hydrogen generation [**10**]. For environmental applications, NTP is used for surface sterilization in order to eliminate bacteria **[11],** for water treatment, and for controlling hazardous air pollutants emitted from solvents, paints, automobile exhaust gas, etc. **[12-14]**

In addition, a variety of dielectric barrier discharge (DBD) plasma reactors have been used for the destruction of various VOCs [**15-21**]. The use of a catalyst in the plasma zone has been reported to improve the efficiency of VOC removal **[22].** Moreover, a synergetic effect can be expected when combining volumic plasma with a photocatalyst **[21, 22].** On the other hand, Ochiai and co-workers investigated and developed a photocatalysis-plasma hybrid air-purification reactor using a titanium mesh sheet modified with TiO_2 (TMiP ^{TM}) and a surface discharge-induced plasma (SPCP) unit [**20**]. In present study, a novel photocatalysis-plasma hybrid is established in a pilot reactor to investigate the influence of some operating parameters on the removal of VOCs in atmospheric conditions. In our system, the surface dielectric barrier type, is generated by a helicoidally wire electrode which maintain the photocatalyst on the inner wall of the reactor, so that the plasma can be formed directly on the surface of the photocatalyst whereas it was simultaneously illuminated by the external UV radiation.

The removal efficiency of isovaleraldehyde by photocatalysis (using external UV) and plasma are tested separately. Isovaleraldehyde (ISOVAL) was chosen since this pollutant is the main molecule detected in the exhaust gases from animal quartering centers.

In this paper, the ISOVAL byproducts are identified and evaluated with DBD plasma, photocatalysis and a DBD plasma/photocatalysis combination. In addition, a possible pathway is proposed.

2. Experimental set-up and conditions

The DBD plasma pilot used (Fig. 1.a) consists of two concentric cylinders (Ø 58 and 76 mm). To generate the DBD plasma, the reactor is covered by a copper grid, which constitutes the outer electrode. The inner electrode is made from a continuous aluminum helix. It is a 2-mm-thick wire electrode, shaped like a coiled spring (12 turns in 250 mm), in close contact with the inner wall of the reactor. The dielectric medium, the glass reactor wall, is 4 mm in thickness (Fig. 1.b). The high electric voltage applied is about 30 kV/40 mA and is a sine waveform. It is delivered by a high voltage amplifier (TREK_30 kV model 30/20A, USA) coupled with a voltage generator (BFi OPTILAS, France). The outer electrode is connected to the ground through a 2.5 nF capacity. The high voltage applied and the voltage across the capacity are visualized using a digital oscilloscope (Lecroy Wave Surfer 24 Xs, 200 MHz) (Fig. 1.b).

The catalytic material, provided by Ahlstrom **[23],** consists of a Glass Fiber Tissue (GFT) coated with 13 $g.m^{-2}$ of colloidal silica to ensure the fixation of 13 $g.m^{-2}$ of titanium dioxide nanoparticles (PC500 Millennium). The coating process involves impregnating the glass fibers with a SiO_2 and TiO_2 nanoparticle suspension in pure water. The preparation process is described in detail in the Ahlstrom Patent [**23**]. The specific surface area was measured according to the BET method and is equal to 20.6 $m^2.g^{-1}$. This material has a thickness of 2 mm. The GFT is maintained on the inner reactor wall by the wire electrode (see Fig. 1.b) so that plasma is generated directly on the catalyst surface. The light source is an 80 W UV lamp with a major wavelength peak emission at 360 nm (Philips CLEO performance). The light tube, 1.5 m in length, is placed in the inner concentric cylinder (Fig. 1.b). The UV intensity, which is measured by a UV radiometer (VLX-3W equipped with a sensor CX 365, ALYS Technologies, Switzerland) at the photocatalyst surface, is equal to 20 ± 3 $W.m^{-2}$.

The design of this reactor (Fig. 1.b) is the subject of a French Patent Application [**24**].

Two sampling points, sealed with a septum, are used to analyze the inlet and outlet gas composition of the reactor. The main air flow can be generated by the internal network of compressed air when dry air is needed (maximum 2 $m^3.h^{-1}$ at 5% relative humidity) or by using ambient air when working at a higher flow rate. The compressed air network enables moisture to be controlled by varying the flow in a packed air-water countercurrent column. Thus, it is possible to obtain a range of relative humidity (RH) from 5 to 90%. The pollutant (ISOVAL) is injected into the inlet air through a syringe pump with a manual refill and a volume of 5 mL. A Venturi system is installed to improve the homogenization of the contaminated air before it is introduced into the reactor. A gas chromatograph coupled with a flame ionization detector (GC Thermo Focus, USA) is used to evaluate the inlet-outlet isovaleraldehyde concentration. ISOVAL and byproduct separation are performed by a Chrompact FFAP-CB column (25 m in length, external diameter of 0.32 mm), which is specially adapted for volatile fatty acids. Nitrogen gas is the mobile phase. Byproducts are identified by a Gas Chromatograph-Mass Spectrometer (GC-MS) (Thermo Scientific) equipped with an infrared (IR) detector. All injections are performed manually and repeated three times with a syringe of 500 µl. Analysis conditions are as follows (Table 1).

Table 1: Analysis conditions for the gas chromatograph

The CO concentrations are measured by an NO/CO ZRE gas analyzer while CO_2 is analyzed by a Transform Infrared Fourier (FTIR) spectrophotometer from Environnement SA (Cosma Beryl reference 100). The measurement accuracy is 5%.

The ozone concentration is determined by the iodometric wet-chemistry method **[25]**.

The experiment is carried out at room temperature and atmospheric pressure**.** The temperature and relative humidity are measured by a TESTO sensor.

A schematic diagram of the experimental system is illustrated in Figures 1.a and 1.b.

Fig. 1.a: Experimental set-up

Fig. 1.b: General scheme for coupled DBD plasma and photocatalysis

3. Results and discussion

The study of ISOVAL removal, the amount of ozone generated and the selectivities of CO and CO_2 was carried out for three reactor configurations (Fig. 1.b): photocatalysis, DBD plasma, and combined DBD plasma/photocatalysis. The influence of some operating parameters on each process performance was investigated. The experiments, which were repeated twice, showed good reproducibility with 5% standard deviation. This is represented by vertical bars in the experimental results in all figures.

Before every experiment, the power was turned off (UV and/or electric discharge) and then, once the inlet and outlet concentrations of VOCs were the same (adsorption equilibrium state), the reactor power was turned on. Output samples were collected at 30- to 60-minute intervals until a steady state was achieved. At the end of the experiment, the reactor was cleaned by a flow of clean air for at least one hour.

3.1. Effect of Specific Energy (SE)

SE is related directly to the energy consumption for the removal of the pollutant. Thus, it can influence the performance of the process.

The plasma-injected energy per cycle (E) is determined by the Lissajous plot method **[26]**, which enables the power input injected (P) as well as the specific energy (SE) to be calculated as follows:

$$P\ (W) = E\ (J) \times \text{frequency}\ (Hz) \quad (1)$$

$$SE\ (J/L) = P\ (W) / Q\ (m^3.s^{-1})/1000 \quad (2)$$

where Q represents the flow rate.

The power value (P) is adjusted by changing the applied voltage (U_a).

3.1.1. On the removal of isovaleraldehyde

The removal capacity of isovaleraldehyde RC ($mg.h^{-1}$) is calculated as:

$$RC = Q.\frac{C_{in}}{100}.IRE(\%) \quad (3)$$

where IRE(%) isovaleraldehyde conversion is defined as:

$$IRE\ (\%) = \frac{C_{in} - C_{out}}{C_{in}} \times 100\ \% \quad (4)$$

where C_{in} and C_{out} are the inlet and outlet pollutant concentrations ($mg.m^{-3}$), respectively and Q is the flow rate ($m^3.h^{-1}$).

Previous experiments have shown the ability of a non-thermal surface plasma discharge to activate the photocatalyst, such as TiO_2 [**27**]. In order to investigate the effect of plasma UV on TiO_2 activity, a study of ISOVAL removal in a DBD plasma reactor in the presence of photocatalyst was carried out without external UV.

Fig. 2: Dependence of SE on ISOVAL removal *in situ* in different plasma systems without external UV.

Fig. 2 shows that ISOVAL removal efficiency is not enhanced in the presence of photocatalyst without external UV. Thus, the UV light generated by the DBD reactor is too weak to activate TiO_2 and its contribution to ISOVAL removal can be ignored. This result is in agreement with work on the removal of the ammonia gas **[20]**.

In contrast, the introduction of external UV light to the plasma significantly improves the IRE. Fig. 3 shows that when SE increases, the IRE increases as well. For example, with plasma alone, when SE is three times greater, the IRE increases from 44 to 76%. The same behavior is observed when DBD plasma is combined with photocatalysis (Fig. 3). This phenomenon is expected as, by increasing the voltage across the reactor, the electric field in the reactor annulus can be enhanced, resulting in a higher degree of ionization **[18, 21-22]**. Therefore, the pollutant is more likely to be attacked by electrons or radicals resulting in a greater removal of ISOVAL.

When only the photocatalysis process is used, the IRE is about 45%.

Fig. 3: Variation of ISOVAL removal efficiency with SE using the three processes (Q = 2 $m^3.h^{-1}$, T = 20 °C, RH = 5%, I = 20 $W.m^{-2}$).

By comparing the IRE (Fig. 3), it is clear that with coupled DBD plasma/photocatalysis and external UV, ISOVAL is easily removed. Moreover, for an inlet concentration of 75 $mg.m^{-3}$, Fig. 3 shows that ISOVAL can be completely removed by coupled DBD plasma/photocatalysis when the SE is higher than 17 $J.L^{-1}$.

In fact, the reactive species generated can efficiently oxidize ISOVAL and thus improve the IRE. Both energetic electrons and atomic oxygen ($O^{\bullet}$) are the main reactive species responsible for ISOVAL removal in the air stream. The number of reactive species can be greatly increased in the presence of a photocatalyst, which explains why combined DBD

plasma/photocatalysis performs better in terms of ISOVAL abatement than DBD plasma alone.

3.1.2. On the selectivity of CO and CO_2

Isovaleraldehyde is mostly converted to CO_2, CO and other organic compounds. The variations of overall CO and CO_2 selectivity are represented in Figure 4. These latter parameters are calculated as follows:

$$\left\{CO_x\ selectivity\ (\%)\right\} = \frac{\left[CO_x\right]_{isov}^{out} - \left[CO_x\right]_{isov}^{in}}{5 \times \left[ISOVAL\right]^{in} \times \left\{\%\ IRE\right\}} \times 10^4 \qquad (5)$$

where x = 1 for CO and x = 2 for CO_2. $[CO_x]^{in}$ and $[CO_x]^{out}$ are the inlet and outlet concentrations of carbon mono/dioxide respectively (ppmv). $[ISOVAL]^{in}$ is the inlet concentration of ISOVAL (ppmv). The number 5 is the stoichiometric coefficient of the removal reaction.

In the first instance, it can be seen (Fig. 4) that CO selectivity can be considered negligible with plasma and coupled DBD plasma/photocatalysis. Certainly, no CO is produced with photocatalysis alone. This result is in agreement with works on the photocatalytic removal of cyclohexane **[13]**, trichloroethylene [**11**] and formaldehyde **[28]**.

Concerning CO_2 selectivity, the increase in SE leads to more mineralization because more electrons and reactive species are produced and thus the ISOVAL byproducts are more mineralized **[29]**. In fact, when SE increases from 9 to 17 $J.L^{-1}$, CO_2 selectivity (with DBD plasma alone) increases from 15 to 39%. It is interesting to note that when DBD plasma is coupled to photocatalysis, CO_2 selectivity varies from 40 to 66%. Consequently, this behavior is due to the photocatalytic activity of TiO_2 in the presence of UV radiation. In fact, when the two processes are combined, carbon dioxide selectivity improves compared to DBD plasma

alone, whatever the value of SE **[26, 30]**. Moreover, some intermediates generated by ISOVAL removal are probably deposited on the photocatalyst surface where mineralization can thus occur **[10]**. This result is similar to many studies reported on acetylene **[26, 31].**

The photocatalysis process is not concerned by SE variation. However, it is interesting to note that this process leads to the best CO_2 selectivity. Many research works confirm that such mineralization improvements are related to the porosity of the medium: porosity induces a longer residence time of gas byproducts during diffusion through the solid pore system [**10, 27, 32, 33**].

Fig. 4: Variation of CO and CO_2 selectivities vs. SE using three processes: empty symbol = selectivity of CO and full symbol = selectivity of CO_2 ([ISOVAL] = 75 mg.m^{-3}, Q = 2 m^3.h^{-1}, T = 20 °C, RH = 5%, I = 20 W.m^{-2}).

On the other hand, in our study, the byproducts are process-dependent. In fact, with photocatalysis, the detected byproducts are propionic acid (CH_3CH_2COOH), acetone (CH_3COCH_3), acetic acid (CH_3COOH) and CO_2.

To evaluate the validity of the analytical method, i.e. to ensure that the majority of byproducts are detected, the carbon balance was estimated. It is equal to the ratio of the sum of carbon byproducts to the isovaleraldehyde removed. Therefore, for combined DBD plasma/photocatalysis, the carbon balance is simply calculated as the sum of the ratios (expressed in percentage) of the number of moles of carbon present in the reaction products relative to their respective moles in the isovaleraldehyde removed.

The carbon balance value is expressed as:

$$CB(\%) = \frac{\sum C_{measured}}{\sum C_{ISOVAL\ removed}} \times 100\% \qquad (6)$$

In order to obtain full insight into the intermediates produced in the reaction process, the residence time was varied by varying the gas flow rate.

Fig. 5.a shows that the carbon balance is achieved at 90%, which means that all the main organic byproducts are released from the reactor. Certainly, there are some minor byproducts cannot be detected.

As can be seen in Fig. 5.a, the byproducts are residence-time-dependent. When this latter parameter increases, more carbon dioxide is formed.

Fig. 5.a Variation of carbon balances and selectivity of CO_2 with residence time using photocatalysis alone ([ISOVAL] = 100 mg.m^{-3}, T = 20 °C, I = 20 W.m^{-2}, RH = 50%).

With combined DBD plasma/photocatalysis, CO appears while with plasma alone, the detected byproducts are CO_2, CO, acetone and acetic acid. Thus, the possible pathway of ISOVAL removal consists of the simultaneous removal of a carboxylic function and creation of an alcohol function **[12, 32-34].** This new function is immediately oxidized into a ketone, initiating a new carboxylic function carried on an 'n – 1' carbon molecule. A degradation pathway is proposed from a literature study and checked through experimental investigations **[35]**. Consequently, the possible pathway of ISOVAL removal is represented in Fig. 5.b.

Fig. 5.b: Possible pathway of ISOVAL removal by coupled plasma/photocatalysis with external UV.

3.1.3. On ozone

Ozone plays an important role during VOC oxidation. The atomic oxygen formed, due to *in situ* decomposition of ozone, interacts with pollutants [**36**].

It can be seen that when SE increases, the quantity of ozone increases too. Moreover, it is interesting to note that the presence of photocatalyst reduces the quantity of ozone in the exit of the reactor. In fact, according to the results of Taranto and co-workers **[37],** UV radiation can favor ozone destruction by the following reaction **[37]:**

$$O_3 + h\nu(254 < \lambda < 350\ nm) \rightarrow O_2 + {}^{\bullet}O \qquad (1)$$

No ozone was found in the exit of our photocatalytic reactor.

3.2. Effect of inlet concentration of isovaleraldehyde

The second important experimental parameter that can influence process performance is the inlet concentration.

3.2.1. On the removal efficiency

Fig. 6 illustrates the variation of the IRE versus inlet concentration ranging from 75 to 200 $mg.m^{-3}$. All experiments were carried out at a constant flow rate (2 $m^3.h^{-1}$), relative humidity (5%) and frequency (50 Hz). The IRE decreases with increasing inlet concentration in all three processes. In the DBD plasma reactor, the IRE falls from 70 to 25% when the inlet concentration increases from 75 to 200 $mg.m^{-3}$.

Many electrons and reactive species (like $O^{\bullet}$ and $OH^{\bullet}$) are needed to remove pollutants from the air stream at a high inlet concentration **[21, 26, 30]**. With photocatalysis alone, the removal efficiency decreases proportionally with inlet concentration. This is due to the availability of the photocatalytic sites at this concentration range **[11, 38, 39].**

Fig. 6.a: Variation of removal efficiency with inlet concentration using three processes (SE = 17 J.L^{-1}, Q = 2 m^3.h^{-1}, T = 20 °C, RH = 5%, I = 20 W.m^{-2}).

Additionally, the synergetic outcome was better demonstrated by comparison of the removal capacities (Table 2), where the RC of the combined system was higher (≈15%) than the sum obtained for individually reactors and independent of SE and inlet concentration (100 and 200 mg.m^{-3}). This indicated that coupling of the photocatalytic and DBD reactors significantly improved removal.

The synergetic effect can be ascribed to:

- several mechanisms occurring when the non-thermal plasma is present since the plasma produces various species such as high-energy electrons, excited molecules or radicals ($O^{\bullet}$, N, $OH^{\bullet}$, $O_2^{\bullet-}$, O_3, NO_2, NO_x, etc.). These molecules can interact directly with ISOVAL molecules.
- plasma promotes the desorption of byproducts attached at the TiO_2 surface and then accelerates the conversion and mineralization **[40]**.
- plasma can induce activation of TiO_2 by creating a hole/electron pairs by ion bombardment **[21, 22, 40]**.

Table.2: RC values for isovaleraldehyde removal by plasma DBD, photocatalysis and a coupled process at different inlet concentrations and specific energies.

3.2.2. On the selectivity of CO and CO_2

Using photocatalysis alone, when the inlet concentration increases, the selectivity of CO_2 decreases (Fig. 7). This means that the quantity of intermediate byproducts generated, except for CO_2, is greater. This behavior is due to the fact that the increase in inlet concentration leads to a lower availability of active sites. Assuming that removal is a series of successive reactions, the competition for the active sites of the catalyst becomes greater when the inlet concentration increases, thus the intermediate byproducts generated cannot be mineralized [**7**,**18, 41, 42**].

Using DBD plasma alone, the low values of overall CO_2 selectivity are explained by the fact that the quantity of reactive species generated becomes insufficient and the chemical reaction is the limiting step. This result is similar to those in the literature for toluene **[43]** and benzene **[18, 44].**

On the other hand, combined DBD plasma/photocatalysis enhances CO_2 selectivity significantly, compared to DBD plasma alone. This is attributed to the formation of more reactive species due to the presence of TiO_2 in the plasma discharge zone. Moreover, UV light is able to activate ozone on the surface of TiO_2 in order to improve mineralization. Consequently, possible pathways for pollutant removal in combined DBD plasma/photocatalysis mainly include gas-phase radical attacks due to various other species such as high-energy electrons, excited molecules or radicals ($O^{\bullet}$, N, $OH^{\bullet}$, $O_2^{\bullet-}$, O_3, NO_2, NO_x, etc.) **[4, 5].**

Fig. 7: Variation of CO and CO_2 selectivities with inlet concentration using three processes: empty symbol represents selectivity of CO and full symbol represents selectivity of CO_2 (SE = 17 J.L^{-1}, Q = 2 m^3.h^{-1}, T = 20 °C, RH = 5%, I = 20 W.m^{-2})

3.2.3. On ozone

Fig. 8 represents ozone production using the three different processes at different inlet concentrations. With DBD plasma alone, increasing the isovaleraldehyde inlet concentration in the air stream from 75 to 200 mg.m^{-3} halves the amount of ozone. The amount of ozone produced is dependent on ISOVAL concentration. This could be due to the plasma process. A similar trend was observed when using the coupled process.

Fig. 8: Variation of amount of ozone with inlet concentration using three processes (SE = 17 J.L^{-1}, Q = 2 m^3.h^{-1}, T = 20 °C, RH = 5%, I = 20 W.m^{-2}).

3.3. Effect of relative humidity

The study of the effect of relative humidity (RH) is of great interest since practical applications deal with ambient air that usually contains large amounts of water.

In order to understand the influence of RH on the IRE and byproduct formation by DBD plasma and photocatalysis, each oxidative configuration was tested separately: (i) photocatalytic oxidation of ISOVAL (ii) DBD plasma oxidation of ISOVAL and (iii) DBD plasma/photocatalysis combination.

3.3.1. On isovaleraldehyde removal

Using photocatalysis alone, it is well known that the presence of water molecules in the air stream leads to the formation of OH• radicals **[28, 39]** which improve the IRE.

Here, the IRE increases and then drops. In fact, when RH increases, the competitive effect towards the active sites of water becomes predominant and thus the IRE decreases. In our

case, an optimum RH value around 50% is seen (Fig. 9). Many other VOCs like trichloroethylene **[45]** and cyclohexane **[13]** show the same behavior toward RH.

Nevertheless, when DBD plasma is used, the influence of water vapor on the IRE is not significant (Fig. 9), regardless of the value of SE. The IRE is around 40% whatever the value of RH at SE equal to 17 $J.L^{-1}$.

With combined DBD plasma/photocatalysis, the IRE increases significantly with increasing RH content up to 60%. Certainly, water vapor content enhances the formation of reactive species as in the equation **[45-46]**:

$$H_2O + e^- \rightarrow H^\bullet + HO^\bullet \quad (2)$$

On the other hand, at higher levels of RH, an inverted trend occurs and the IRE becomes slightly lower. This is because the increased water vapor content limits the electron density and quenches the active chemical species **[4, 5].** This behavior is similar to that reported in the literature for some VOCs **[44-46].**

Fig. 9: Variation of IRE vs. RH using three processes ($[ISOVAL]_0$ = 100 $mg.m^{-3}$, Q = 2 $m^3.h^{-1}$, T = 20 °C, SE = 17 $J.L^{-1}$, I = 20 $W.m^{-2}$).

Moreover, as shown in Table 3 the variation of RH does not affect the synergistic effect in combined DBD plasma/photocatalysis. In fact, at each value of RH, the RC due to the combined process is higher than the value corresponding to the sum of the removal capacities of each process taken separately.

Table.3: RC values for isovaleraldehyde removal by plasma DBD, photocatalysis and a coupled process at different RH.

3.3.2. On the selectivities of CO and CO_2

As shown on Fig. 10, water vapor has a significant effect on CO_2 selectivity. In fact, when RH increases from 5 to 90%, with DBD plasma alone, CO_2 selectivity increases from 31 to 48%. As previously described, a small amount of water vapor is essential for the formation of active species (such as $OH^{\bullet}$ and $O^{\bullet}$) which leads to more mineralization of byproducts. Additionally, it is interesting to note that there is no CO when RH is equal to 90%.

With photocatalysis alone, when RH increases from 5 to 60%, CO_2 selectivity remains stable. However, a further increase in RH reduces mineralization. This behavior arises because water vapor can deposit on the surface of the photocatalyst and occupy its active sites. If the number of active sites is considered constant, it becomes evident that the competitive effect increases with increasing RH.

With coupled plasma DBD plasma/photocatalysis, CO_2 selectivity increases by about 20% compared to DBD plasma alone (Fig. 10). For the above reason, it might be concluded that the photocatalyst leads to more ISOVAL mineralization because the presence of $OH^{\bullet}$ radicals greatly improves the oxidation of CO into CO_2 [**48**]. This result is similar to that found in the literature for acetylene **[48]**. In fact, several authors **[48]** have reported that CO and CO_2 are related by an equilibrium reaction under plasma action. Moreover, Futamura et al. **[49]** take this equilibrium between CO and CO_2 into account and suggest that the presence of $OH^{\bullet}$ radicals shifts the equilibrium towards the formation of CO_2.

Fig. 10: Variation of the overall selectivity of CO_2 vs. RH

([ISOVAL] = 100 $mg.m^{-3}$, Q = 2 $m^3.h^{-1}$, T = 20 °C, SE = 17 $J.L^{-1}$, I = 20 $W.m^{-2}$).

3. 3. 3. On ozone

The results of ozone production at different RH are reported in Fig. 11. With DBD plasma alone, ozone is strongly reduced when RH increases (Fig. 11). Its formation is probably inhibited. For example, the quantity of ozone is reduced three times when RH increases from 30 to 60-65%.

Fig. 11: Variation of the amount of ozone with RH using three processes ($[ISOVAL]_0$ = 100 mg.m^{-3}, Q = 2 m^3.h^{-1}, T = 20 °C, SE = 17 J.L^{-1}, I = 20 W.m^{-2}).

The consumption of ozone in the presence of radicals ($H^\bullet + HO^\bullet$) can be explained by these two reactions [**50, 51**]:

$$O_3 + OH^\bullet \rightarrow O_2 + HO_2^\bullet \quad (3)$$

$$O_3 + H^\bullet \rightarrow O_2 + HO^\bullet \quad (4)$$

Similar trends were observed for coupled DBD plasma/photocatalysis.

Conclusion

Many parameters were investigated in this work such as SE, inlet concentration of isovaleraldehyde and RH. Their influences on the performances of three processes (DBD plasma, photocatalysis and combined DBD plasma/photocatalysis) were studied.

An increase in inlet concentration greatly modifies the oxidative processes: (i) the IRE is considerably slowed down; (ii) the mineralization of ISOVAL is reduced. However, increasing SE improves both the IRE and mineralization of ISOVAL.

Water vapor plays a very important role in the elimination of ISOVAL. An optimum RH value is observed with photocatalysis alone and with the combined process. Water vapor also

improves CO_2 selectivity and decreases the amount of CO. On the other hand, RH reduces ozone formation.

For each operating parameter, we have shown unambiguously that a synergetic effect on ISOVAL removal can be observed when DBD plasma is coupled with TiO_2 catalyst irradiated by external UV.

Moreover, the byproducts of DBD plasma, photocatalysis and combined DBD plasma/photocatalysis have been identified and evaluated. A possible pathway for ISOVAL removal is proposed.

Acknowledgments

The authors wish to thank the French National Research Agency (ANR) for supporting this research. They also thank the Ahlstrom Company for providing the photocatalytic medium.

References

[1] B. Eliasson, W. Egli and U. Kogelschatz, Modelling of dielectric barrier discharge chemistry, Pure & Appl. Chsm., 66 (1994) 1275-1286.

[2] ADEME, 2005. Pollutions olfactives : origine, législation, analyse, traitement, Ademe, Dunod, Angers.

[3] P. Le Cloirec, 1998. Les composés organiques volatils (COV) dans l'environnement, Lavoisier, Tec&Doc, Paris.

[4] H. Huang, D. Ye, D. Y. C. Leung, Plasma-driven catalysis process for toluene abatement: effect of water vapor, IEEE Transactions on Plasma Science, 39 (2011) 576 – 580.

[5] H. Huang, D. Yea, D. Y. C. Leung, F. Feng, X. Guan, Byproducts and pathways of toluene destruction via plasma-catalysis, Journal of Molecular Catalysis A: Chemical 336 (2011) 87–93.

[6] P. Monneyron, M. H. Manéro, S. Mathe, A combined selective adsorption and ozonation process for VOCs removal from air, The Canadian Journal of Chemical Engineering 85 (2007) 326-332.

[7] T. Ochiai, T. Hoshi, H. Slimen, K. Nakata, T. Murakami, H. Tatejima, Y. Koide, A. Houas, T. Horie, Y. Morito, A. Fujishima, Fabrication of TiO_2 nanoparticles impregnated titanium mesh filter and its application for environmental purification unit, Catal. Sci. Technol. 1 (2011) 1324–1327

[8] T. Ochiai, K. Nakata, T. Murakami, T. Horie, Y. Morito, A. Fujishima, Anodizing effects of titanium-mesh surface for fabrication of photocatalytic air purification filter, Nanosci. Nanotechnol. Lett. 4 (2012) 544–547.

[9] S. Yao, E. Suzuki and A. Nakayama, a novel pulsed plasma for chemical conversion. Thin Solid Films, 390 (2001) 165-169.

[10] S. Futamura, H. Kabashima and G. Annadurai, Roles of CO_2 and H_2O as oxidants in the plasma reforming of aliphatic hydrocarbons. Catalysis Today 115 (2006) 211–216.

[11] R. Ben Gadri, J. R. Roth, T. C. Montie, K. Kelly-Wintenberg, P P.-Y. Tsai, D. J. Helfritch, P. Feldman, D. M. Sherman, F. Karakaya, Zh.u Chen, Sterilization and plasma processing of room temperature surfaces with a one atmosphere uniform glow discharge plasma OAUGDP Surface and Coatings Technology 131 (2000) 528-542.

[12] H. H. Kim, K. Takashima, S. Katsura , A. Mizuno,., Low-temperature NOx reduction processes using combined systems of pulsed corona discharge and catalysts, J. Phys. D : Appl. Phys., 34 (2001) 604-613.

[13] Y. S. Mokt, H. W. Lee, Y. J. Hyun, S. W. Ham, I.-S. Nam, Determination of Decomposition Rate Constants of Volatile Organic Compounds and Nitric Oxide in a Pulsed Corona Discharge Reactor, Korean J. Chem. Eng, 18 (2001) 711-718.

[14] M. Derakhshesh, J. Abedi, H. Hassanzadeh, Mechanism of methanol decomposition by non-thermal plasma, Journal of Electrostatics 68 (2010) 424-428.

[15] S. Delagrange, L. Pinard, J.-M. Tatibouet, Combination of a non-thermal plasma and a catalyst for toluene removal from air: Manganese based oxide catalysts, Applied Catalysis B: Environmental 68, (2006) 92–98.

[16] A. A. Assadi, A. Bouzaza, M. Lemasle, D. Wolbert, Removal of trimethylamine and isovaleric acid from gas streams in a continuous flow surface discharge plasma reactor, Chemical Engineering Research and Design, in press.

[17] K. Allegraud. Décharge à Barrière Diélectrique de Surface : physique et procédé, thèse Ecole polytechnique de Paris, 2008.

[18] H.M. Lee, M.B. Chang, Gas-phase removal of acetaldehyde via packed-bed dielectric barrier discharge reactor, Plasma Chem. Plasma Process. 21(2001) 329-343.

[19] Ch. Subrahmanyama, A. Renken, L. Kiwi-Minsker, Catalytic non-thermal plasma reactor for abatement of toluene, Chemical Engineering Journal, 160 (2010) 677–682.

[20] T. Ochiai, K. Nakata, T. Murakami, Y. Morito, S. Hosokawa, A. Fujishima, Development of an air-purification unit using a photocatalysis-plasma hybrid reactor, Electrochemistry 79 (2011) 838–841

[21] J. Chen, Zh. Xie, Removal of H_2S in a novel dielectric barrier discharge reactor with photocatalytic electrode and activated carbon fiber, Journal of Hazardous Materials 261 (2013) 38–43

[22] T. Ochiai, Y. Hayashi, M. Ito, K. Nakata, T. Murakami, Y. Morito, A. Fujishima, An effective method for a separation of smoking area by using novel photocatalysis-plasma synergistic air-cleaner, Chemical Engineering Journal 209 (2012) 313–317.

[23] Ahlstrom Patent EP 1069950, 2000. AU 735798 US 09/467, 650; JP 2000-542104.

[24] CIAT Patent, Dispositif, système et procédé de traitement de gaz, 2013, EP 1000180221, BFF11L1041/MFH.

[25] R. Atkinson, D. L. Baulch, R. A. Cox, J. N. Crowley, R. F. Hampson, R. G. Hynes, M. E. Jenkin, M. J. Rossi, J. Troe. Evaluated kinetic and photochemical data for atmospheric chemistry: Part 1 - gas phase reactions of Ox, HOx, NOx and Sox species. Atmospheric Chemistry and Physics Discussions, 3 (2003) 6179–6699.

[26] T. C. Manley, 1943. Proceedings of the 84th General Meeting, New York.

[27] O. Guaitella, F. Thevenet, E. Puzenat, C. Guillard, A. Rousseau, C_2H_2 oxidation by plasma/TiO_2 combination: Influence of the porosity, and photocatalytic mechanisms under plasma exposure, Applied Catalysis B: Environmental, 80 (2008) 296–305.

[28] T. N. Obee, R. T. Brown, TiO_2 photocatalysis for indoor air applications: effects of humidity and trace contaminant levels on the oxidation rates of formaldehyde, toluene, and 1, 3-butadiene, Environmental Science and Technology. 29 (1995)1223-1231.

[29] A. M. Vandenbroucke, R. Morent, , N. De Geyter, Ch. Leys, Non-thermal plasmas for non-catalytic and catalytic VOC abatement, Journal of Hazardous Materials 195 (2011) 30–54.

561 [30] O. Guaitella, C. Lazzaroni, D. Marinov, A. Rousseau, Evidence of atomic adsorption on TiO_2 under plasma
562 exposure and related C_2H_2 surface reactivity, Applied Physics Letters, 97 (2010) 011502 (0) - 011502 (3)
563
564 [31] H. B. Huang, D. Q. Ye, M. L. Fu, F. D. Feng., contribution of UV light to the decomposition of toluene in
565 dielectric barrier discharge plasma/photocatalysis system, Plasma Chem. Plasma Process 27 (2007) 577–588.
566
567 [32] A. A. Assadi, A. Bouzaza, D. Wolbert, P. Petit, Isovaleraldehyde elimination by UV/TiO_2 photocatalysis:
568 comparative study of the process at different reactors configurations and scales, Environmental Science and
569 Pollution Research in press.
570 [33] D. D. Dionysiou, M. T. Suidan, I. Baudin, J.-M. Lainé, Oxidation of organic contaminants in a rotating disk
571 photocatalytic reactor: reaction kinetics in the liquid phase and the role of mass transfer based on the
572 dimensionless Damköhler number, Applied Catalysis B: Environmental 38 (2002) 1–16.
573
574 [34] A. A. Assadi, J. Palau, Bouzaza A., D. Wolbert, A continuous air reactor for photocatalytic degradation of
575 Isovaleraldehyde: Effect of different operating parameters and chemical degradation pathway. Chemical
576 Engineering Research and Design 91 (2013) 1307–1316
577
578 [35] B. Boulinguiez, A. Bouzaza, S. Merabet, D. Wolbert. Photocatalytic degradation of ammonia and butyric
579 acid in plug-flow reactor: Degradation kinetic modeling with contribution of mass transfer, Journal of Chemistry
580 and Photobiology A: Chemistry 200 (2008) 254–261.
581
582 [36] H. Wang, D. Li, Y. Wu, J. Li, L. Guofeng, Removal of four kinds of volatile organic compounds mixture in
583 air using silent discharge reactor driven by bipolar pulsed power, Journal of Electrostatics 67 (2009) 547–555.
584
585 [37] J. Taranto, D. Frochot, P. Pichat, Combining Cold Plasma and TiO_2 Photocatalysis To Purify Gaseous
586 Effluents: A Preliminary Study Using Methanol-Contaminated Air, Ind. Eng. Chem. Res. 46 (2007) 7611-7614.
587
588 [38] A. Queffeulou, L. Geron, E. Schaer, Prediction of photocatalytic air purifier apparatus performances with a
589 CFD approach using experimentally determined kinetic parameters, Chemical Engineering Science. 65 (2010)
590 5067–5074.

[39] T. Ochiai, A. Fujishima, Photoelectrochemical properties of TiO_2 photocatalyst and its applications for environmental purification, Journal of Photochemistry and Photobiology C: Photochemistry Reviews 13 (2012) 247–262.

[40] L. Sivachandiran, F. Thevenet, A. Rousseau, Non-Thermal Plasma Assisted Regeneration of Acetone Adsorbed TiO_2 Surface, Plasma Chem. Plasma Process 33 (2013) 855–871.

[41] Ch.-L. Chang, T.-Sh. Lin, Decomposition of Toluene and Acetone in Packed Dielectric Barrier discharge Reactor, Plasma Chemistry and Plasma Processing, 25 (2005) 227-243.

[42] N. Harada, T. Matsuyama, H. Yamamot, Decomposition of volatile organic compounds by a novel electrode system integrating ceramic filter and SPCP method, Journal of Electrostatics, 65 (2007) 43–53.

[43] D. Li, D. Yakushiji, S. Kanazawa, T. Ohkubo, Y. Nomoto, Decomposition of toluene by streamer corona discharge with catalyst, J. Electrostat., 55 (2002) 311-319.

[44] B. Y. Lee, S. H. Park, S.C. Lee, M. Kang, S.-J. Choung, Decomposition of benzene by using a discharge plasma–photocatalyst hybrid system, Catal. Today, 93 (2004) 769-776.

[45] K. H. Wang, H. H. Tsai, Y. H. Hseieh, The kinetics of photocatalytic degradation of trichloroethylene in gas phase over TiO_2 supported on glass bead, Appl. Catal. B: Environ. 17 (1998) 313–320.

[46] Y. Guo, X. Liao, D. Ye, Detection of hydroxyl radical in plasma reaction on toluene removal Journal of Environmental Sciences, 20 (2008) 1429–1432.

[47] Z. Bo, J. H. Yan, X. D. Li, Y. Chi, K. F. Cen, B. G. Cheron, Effects of oxygen and water vapor on volatile organic compounds decomposition using gliding arc gas discharge, Plasma Chem. Plasma Process., 275 (2007) 546–558,

620 [48] F. Thevenet, O. Guaitella, E. Puzenat, C. Guillard, A. Rousseau, 2008. Influence of water vapour on
621 plasma/photocatalytic oxidation efficiency of acetylene, Applied Catalysis B: Environmental, 84 (2008) 813–
622 820.
623
624 [49] J. Chen, Effect of relative humidity on electron distribution and ozone production by DC coronas in air,
625 IEEE transactions on plasma science, 33 (2005) 808-812.
626
627 [50] S. Futamura, A. H. Zhang, T. Yamamoto, The dependence of nonthermal plasma behavior of VOCs on their
628 chemical structures Journal of Electrostatics, 42 (1997) 51-62
629
630
631
632
633
634
635
636
637
638
639
640
641
642
643
644
645
646
647
648
649

Table:

Table 1: Analysis conditions for the gas chromatograph

Table 2: RC values ($mg.h^{-1}$) for isovaleraldehyde removal by DBD plasma, photocatalysis and a coupled process at different inlet concentrations and specific energies ($Q = 2\ m^3.h^{-1}$, $T = 20$ °C, $RH = 5\%$, $I = 20\ W.m^{-2}$).

Table 3: RC values ($mg.h^{-1}$) for isovaleraldehyde removal by DBD plasma, photocatalysis and a coupled process at different relative humidity ($Q = 2\ m^3.h^{-1}$, $T = 20$ °C, $I = 20\ W.m^{-2}$).

Gas pressure			Zone temperature	
N_2 (gas carrier, kPa)	H_2 (kPa)	Air (kPa)	Injector (°C)	Oven (°C)
105	40	100	110	50

Table 1: Analysis conditions for the gas chromatograph

	Inlet concentration	100 mg.m^{-3}	200 mg.m^{-3}
	Photocatalysis	59.80	84.00
SE= 5J/L	DBD plasma	37.87	37.60
	Coupled process	126.6	180.05
SE= 9J/L	DBD plasma	58.00	59.02
	Coupled process	133.2	223.60
SE= 11J/L	DBD plasma	64.39	76.48
	Coupled process	143.8	261.61
SE=17J/L	DBD plasma	79.80	93.20
	Coupled process	171.8	309.43

Table 2: RC values (mg.h^{-1}) for isovaleraldehyde removal by DBD plasma, photocatalysis and a coupled process at different inlet concentrations and specific energies (Q = 2 m^3.h^{-1}, T = 20 °C, RH = 5%, I = 20 W.m^{-2})

	Specific energy	SE=9J.L^{-1}	SE=17J.L^{-1}
RH= 25%	Photocatalysis	63.04	
	DBD plasma	73.47	82.00
	Coupled process	133.8	178.80
RH=60%	Photocatalysis	70.04	
	DBD plasma	64.00	85.02
	Coupled process	148.68	189.20
RH=90%	Photocatalysis	58.10	
	DBD plasma	56.05	71.60
	Coupled process	130.40	158.08

Table 3: RC values (mg.h^{-1}) for isovaleraldehyde removal by DBD plasma, photocatalysis and a coupled process at different relative humidity (Q = 2 m^3.h^{-1}, T = 20 °C, I = 20 W.m^{-2})

Figures:

Fig. 1.a: Experimental set-up.

Fig. 1.b: General scheme for coupled non-thermal plasma and photocatalysis.

Fig. 2: Dependence of SE on ISOVAL removal *in situ* in different plasma systems without external UV.

Fig. 3: Variation of ISOVAL removal efficiency with SE using the three processes (Q = 2 $m^3.h^{-1}$, T = 20 °C, RH = 5%, I = 20 $W.m^{-2}$).

Fig. 4: Variation of CO and CO_2 selectivities vs. specific energy using three processes: empty symbol = selectivity of CO and full symbol = selectivity of CO_2 ([ISOVAL] = 75 $mg.m^{-3}$, Q = 2 $m^3.h^{-1}$, T = 20 °C, RH = 5%, I = 20 $W.m^{-2}$).

Fig. 5.a: Variation of carbon balances and selectivity of CO_2 with residence time using photocatalysis alone ([ISOVAL] = 100 $mg.m^{-3}$, T = 20 °C, I = 20 $W.m^{-2}$, RH = 50%).

Fig. 5.b: Possible pathway of ISOVAL removal by coupled DBD plasma/photocatalysis with external UV.

Fig. 6: Variation of removal efficiency with inlet concentration using three processes (SE = 17 $J.L^{-1}$, Q = 2 $m^3.h^{-1}$, T = 20 °C, RH = 5%, I = 20 $W.m^{-2}$).

797 Fig. 7: Variation of CO and CO_2 selectivities with inlet concentration using three processes: empty
798 symbol represents selectivity of CO and full symbol represents selectivity of CO_2 (SE = 17 $J.L^{-1}$, Q = 2
799 $m^3.h^{-1}$, T = 20 °C, RH = 5%, I = 20 $W.m^{-2}$).
800
801 Fig. 8: Variation of the amount of ozone with inlet concentration using three processes (SE = 17 $J.L^{-1}$,
802 Q = 2 $m^3.h^{-1}$, T = 20 °C, RH = 5%, I = 20 $W.m^{-2}$).
803
804 Fig. 9: Variation of isovaleraldehyde removal efficiency vs. RH using three processes ($[ISOVAL]_0$ =
805 100 $mg.m^{-3}$, Q = 2 $m^3.h^{-1}$, T = 20 °C, SE = 17 $J.L^{-1}$, I = 20 $W.m^{-2}$).
806
807 Fig. 10: Variation of the overall selectivity of CO_2 vs. RH ([ISOVAL] = 100 $mg.m^{-3}$, Q = 2 $m^3.h^{-1}$, T =
808 20 °C, SE = 17 $J.L^{-1}$, I = 20 $W.m^{-2}$).
809
810 Fig. 11: Variation of the amount of ozone with relative humidity using three processes ($[ISOVAL]_0$ =
811 100 $mg.m^{-3}$, Q = 2 $m^3.h^{-1}$, T = 20 °C, SE = 17 $J.L^{-1}$, I = 20 $W.m^{-2}$).
812
813
814
815
816
817

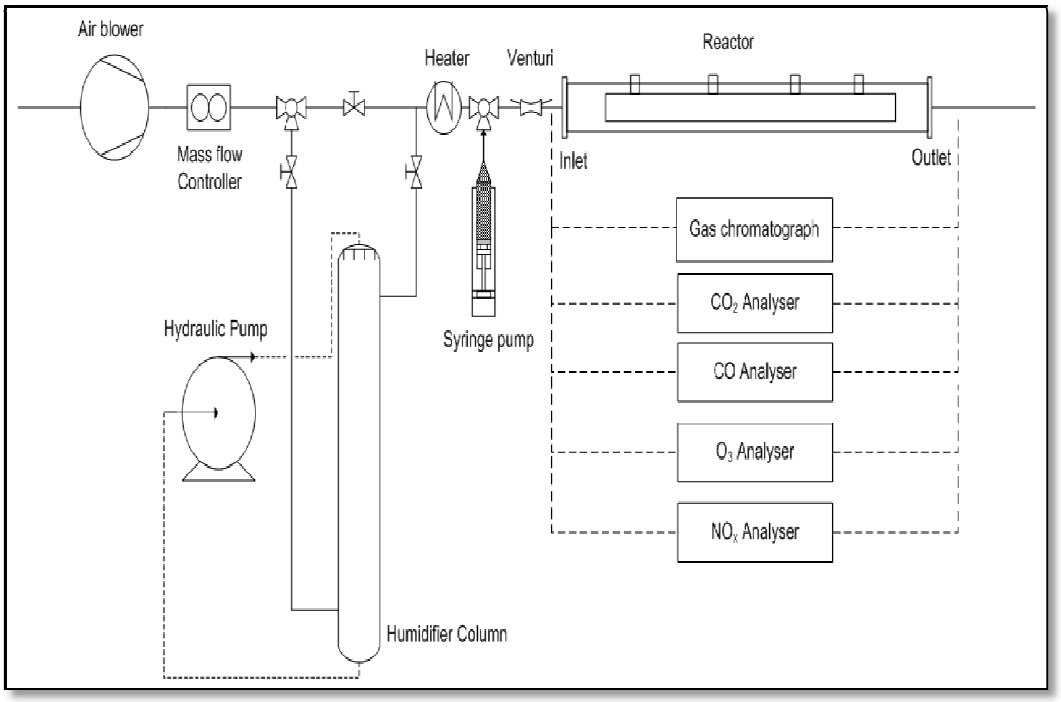

Fig. 1.a: Experimental set-up.

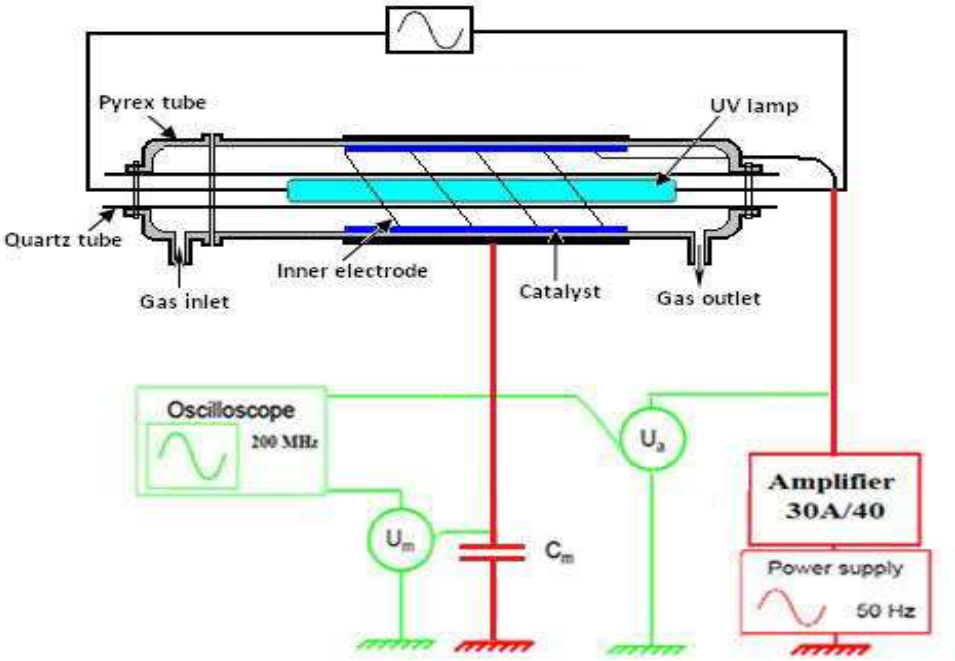

828

829

830 Fig. 1.b: General scheme for coupled non-thermal plasma and photocatalysis.

831

832

833

834

835

836

837

838

839

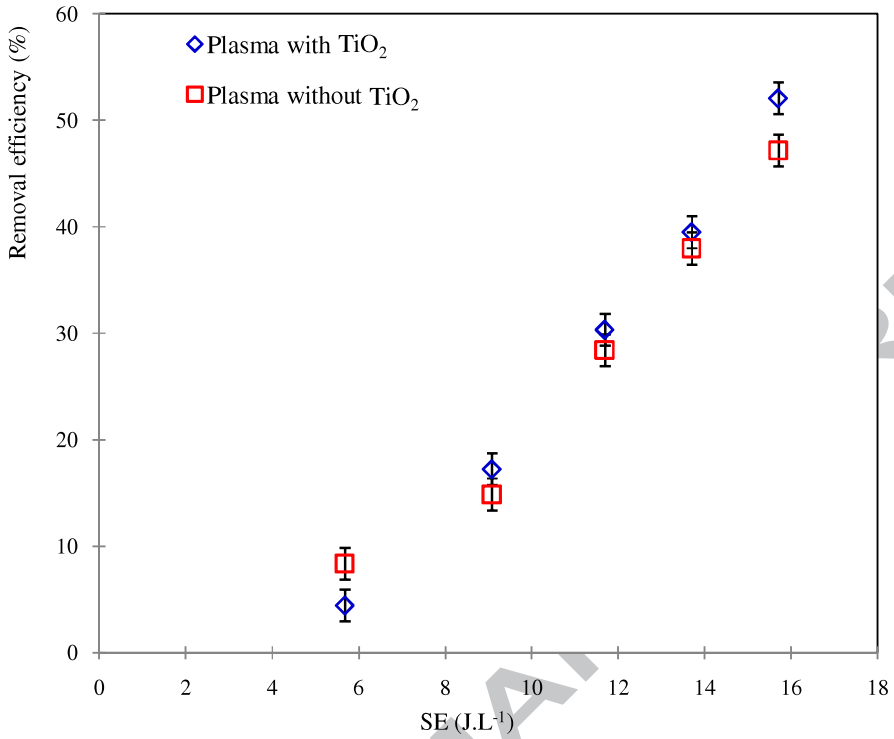

840

841 Fig. 2: Dependence of SE on ISOVAL removal *in situ* in different plasma systems without

842 external UV ([ISOVAL] = 100 mg.m^{-3}, Q = 1 m^3.h^{-1}, T = 20 °C, RH = 5%, I = 20 W.m^{-2}).

843

844

845

846

847

848

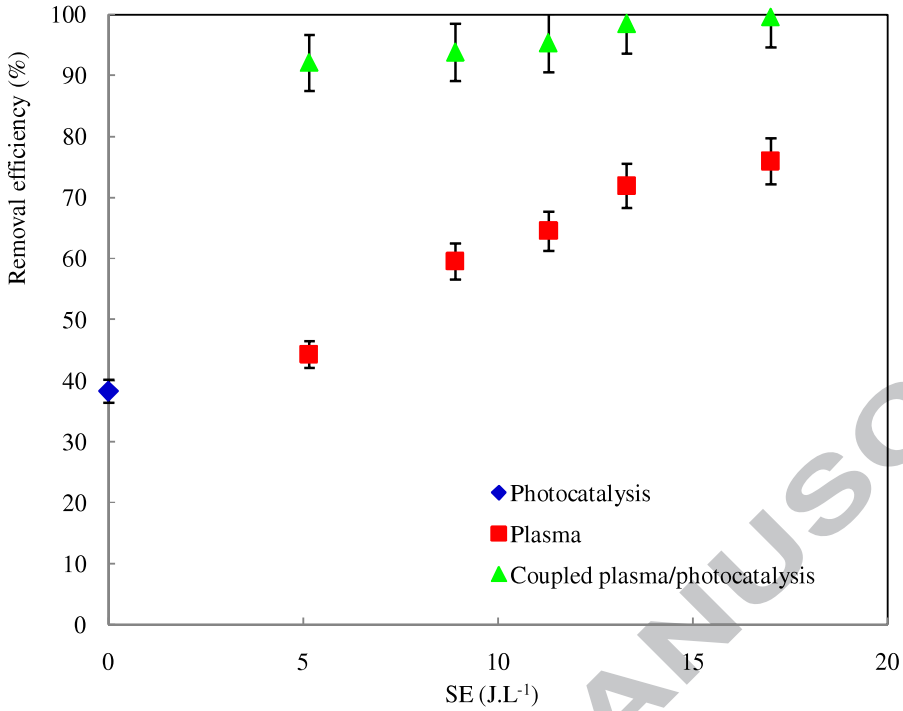

Fig. 3: Variation of ISOVAL removal efficiency with SE using the three processes ([ISOVAL] = 75 mg.m^{-3}, Q = 2 m^3.h^{-1}, T = 20 °C, RH = 5%, I = 20 W.m^{-2}).

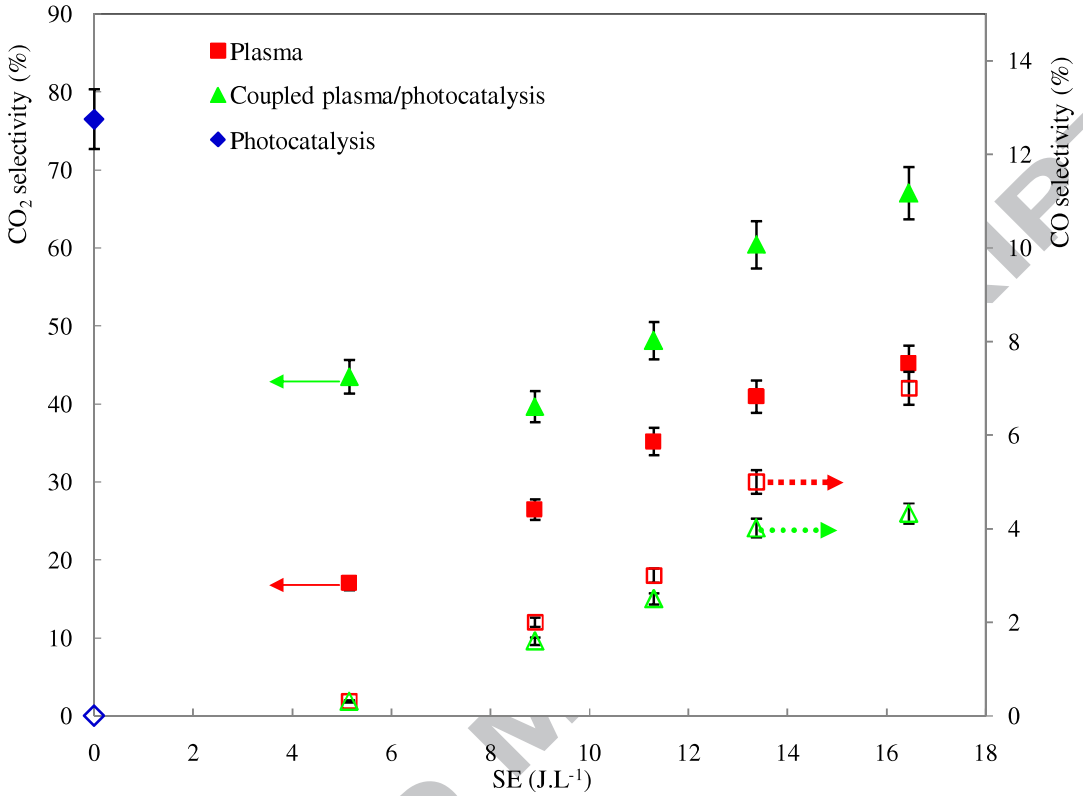

Fig. 4: Variation of CO and CO_2 selectivities vs. SE using three processes: empty symbol = selectivity of CO and full symbol = selectivity of CO_2 ([ISOVAL] = 75 $mg.m^{-3}$, Q = 2 $m^3.h^{-1}$, T = 20 °C, RH = 5%, I = 20 $W.m^{-2}$).

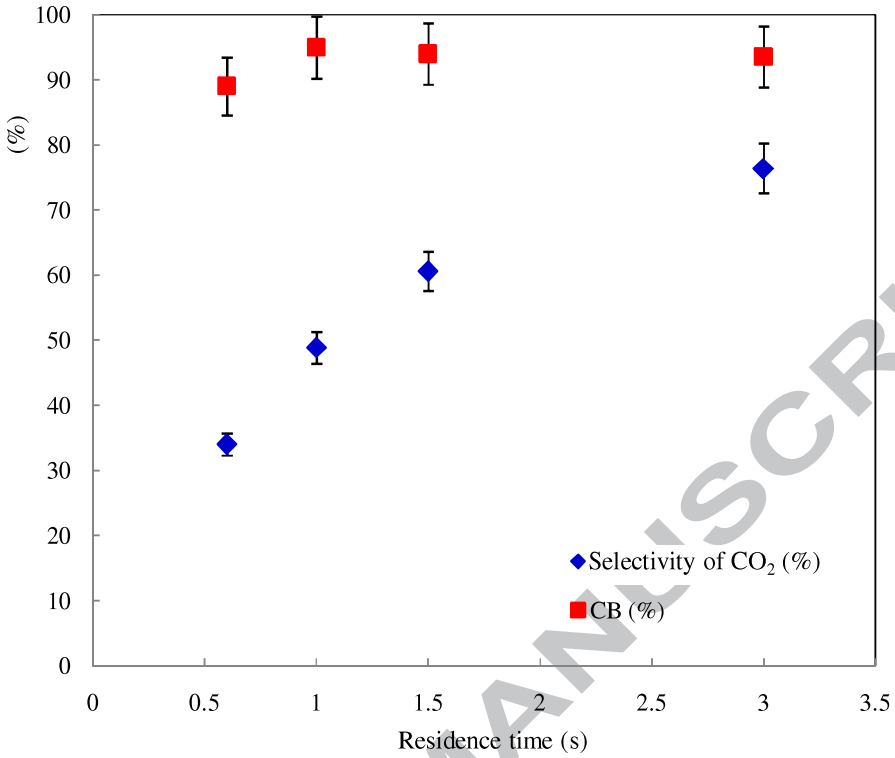

Fig. 5.a: Variation of carbon balances and selectivity of CO_2 with residence time using photocatalysis alone ([ISOVAL] = 75 mg.m^{-3}, T = 20 °C, I = 20 W.m^{-2}, RH = 5%).

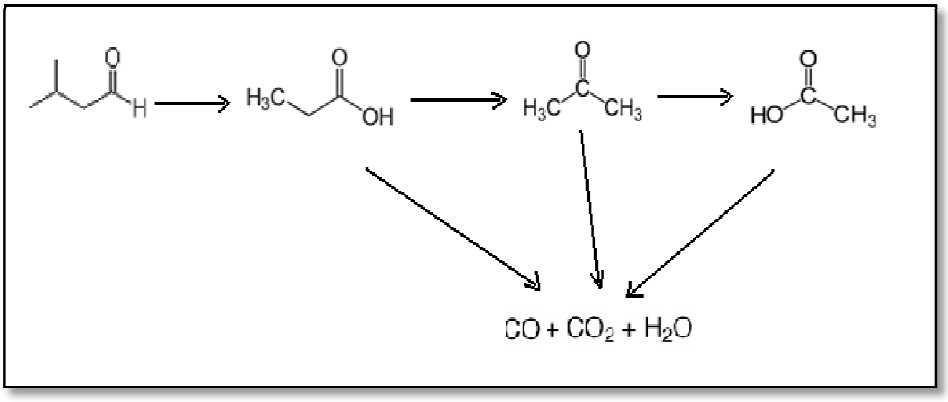

Fig. 5.b: Possible pathway of ISOVAL removal by coupled DBD plasma/photocatalysis.

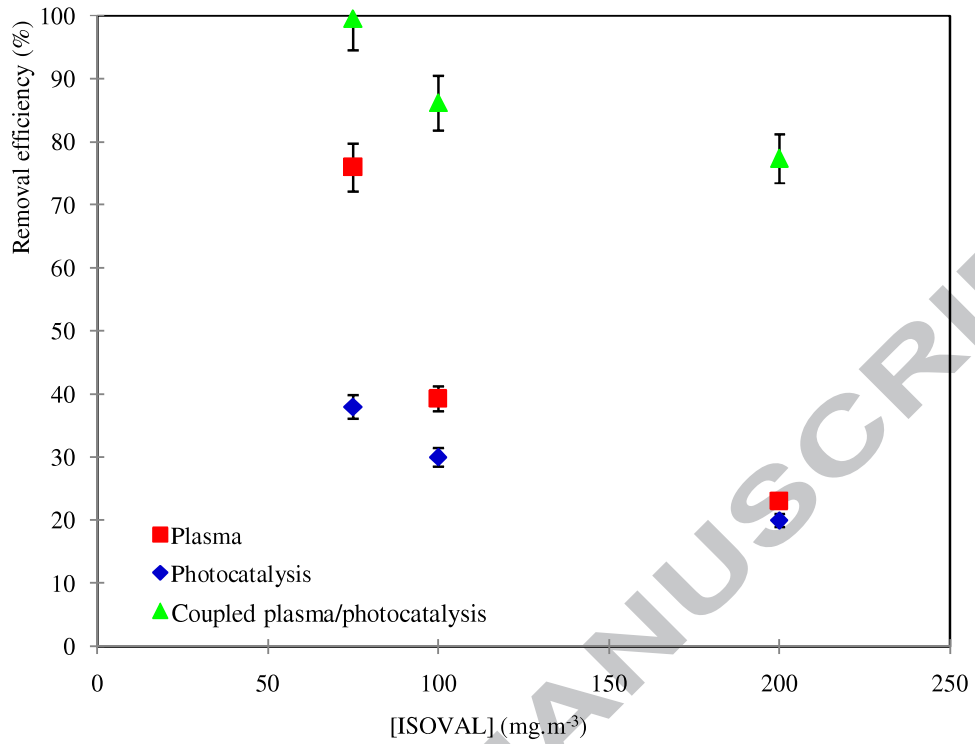

Fig. 6: Variation of removal efficiency with inlet concentration using three processes (SE = 17 $J.L^{-1}$, Q = 2 $m^3.h^{-1}$, T = 20 °C, RH = 5%, I = 20 $W.m^{-2}$).

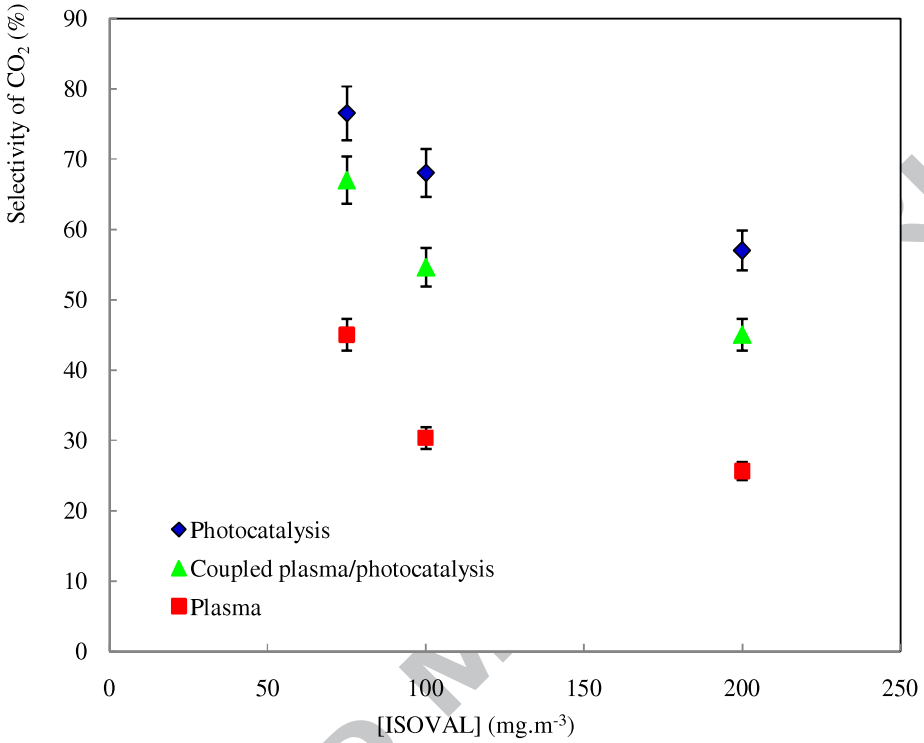

Fig. 7: Variation of CO_2 selectivities with inlet concentration using three processes: (SE = 17 J.L^{-1}, Q = 2 m^3.h^{-1}, T = 20 °C, RH = 5%, I = 20 W.m^{-2}).

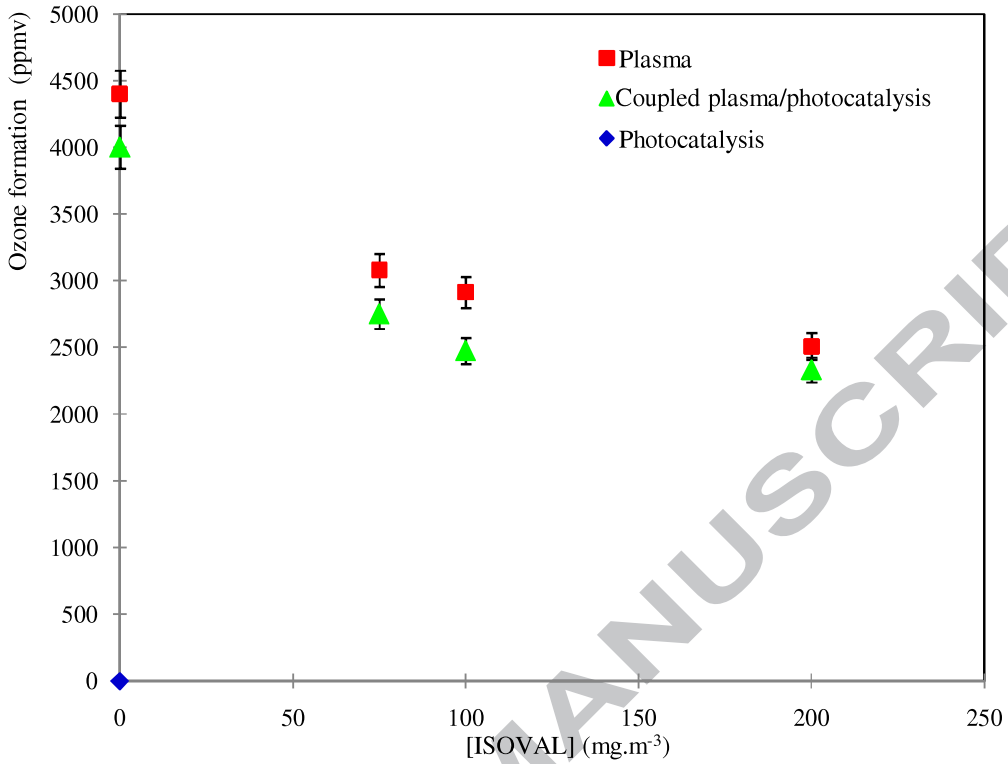

Fig. 8: Variation of the amount of ozone with inlet concentration using three processes (SE = 17 $J.L^{-1}$, Q = 2 $m^3.h^{-1}$, T = 20 °C, RH = 5%, I = 20 $W.m^{-2}$).

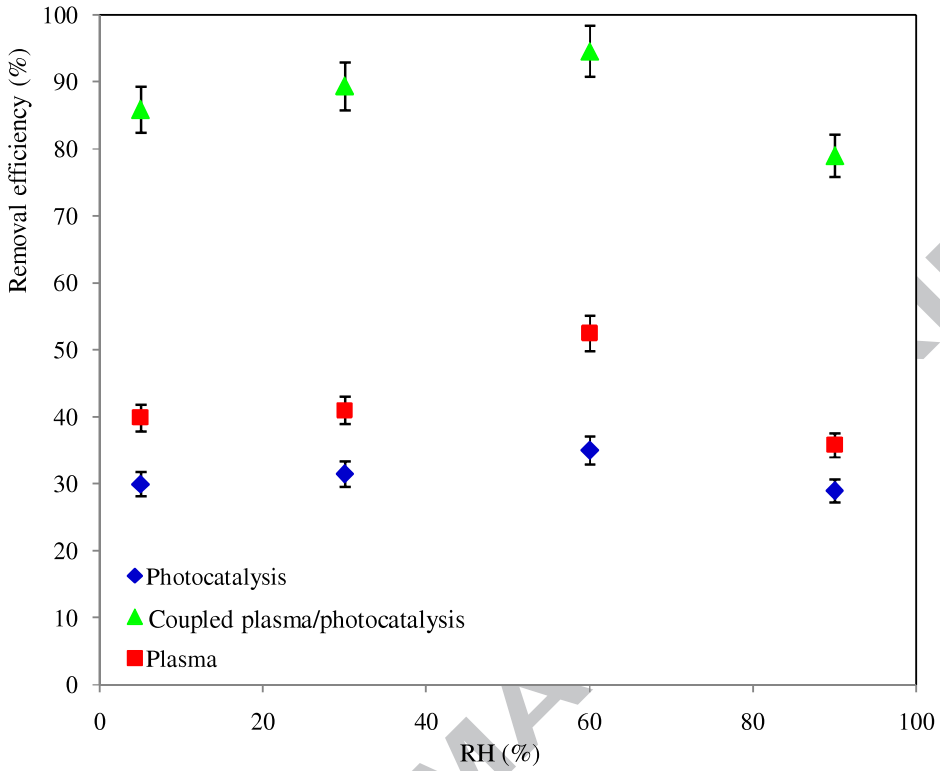

Fig. 9: Variation of isovaleraldehyde removal efficiency vs. RH using three processes ([ISOVAL]$_0$ = 100 mg/m^3, Q = 2 m^3.h^{-1}, T = 20 °C, SE = 17 J.L^{-1}, I = 20 W.m^{-2}).

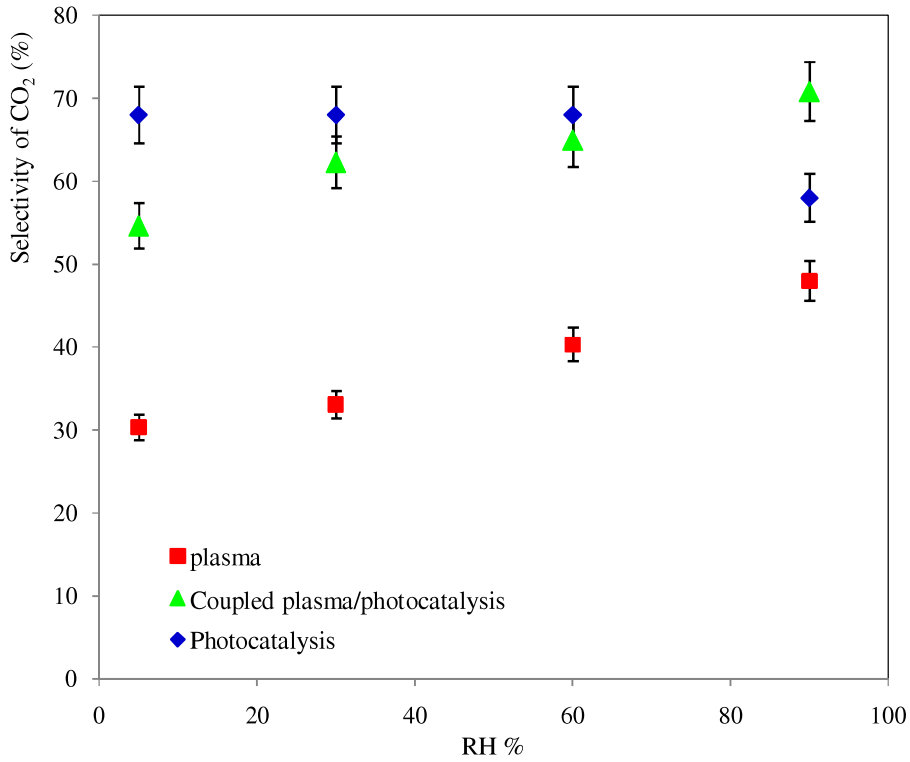

Fig. 10: Variation of the selectivity of CO_2 vs. RH

([ISOVAL] = 100 mg. m^{-3}, Q = 2 $m^3.h^{-1}$, T = 20 °C, SE = 17 $J.L^{-1}$, I = 20 W. m^{-2}).

997

998

999

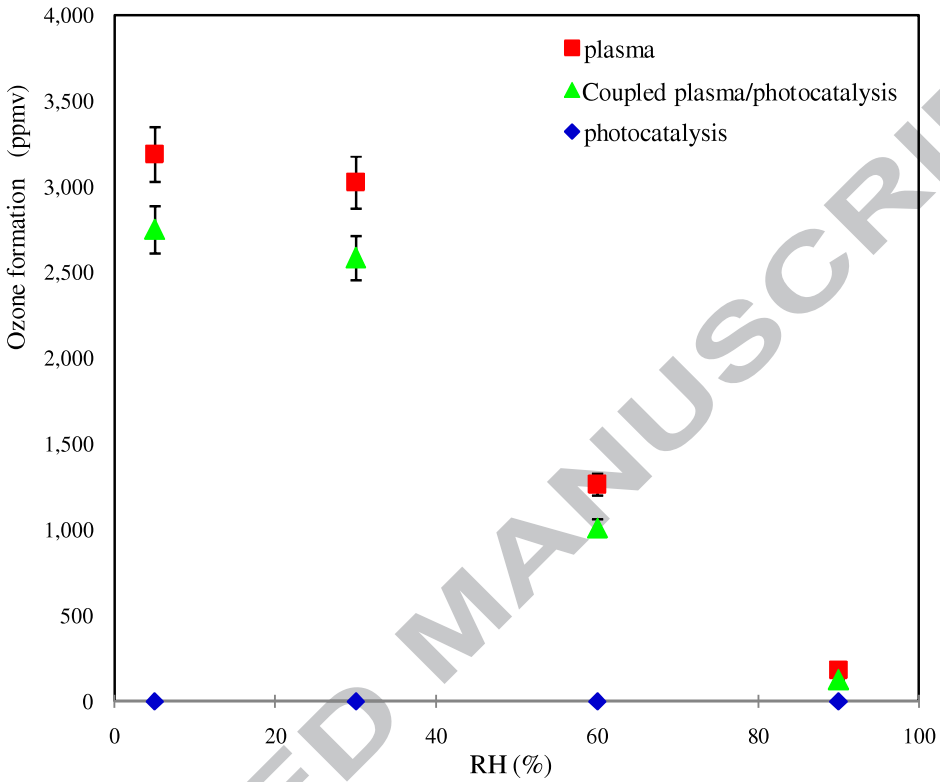

1000

1001 Fig. 11: Variation of the amount of ozone with relative humidity using three processes

1002 ([ISOVAL] = 100 mg. h^{-1}, Q = 2 $m^3.h^{-1}$, T = 20 °C, SE = 17 $J.L^{-1}$, I = 20 W. m^{-2}).

1003

1004

1005

Highlights:

- Isovaleraldehyde elimination by DBD plasma and photocatalysis is studied.
- Effects of some operating parameters on performance of each process are tested.
- A synergetic effect is observed by coupling plasma DBD and photocatalysis.
- The byproducts of isovaleraldehyde are identified and evaluated.
- A possible pathway of Isovaleraldehyde removal is proposed.